Determination of the 15 N chemical shift anisotropy in natural abundance samples by proton-detected 3D solid-state NMR under ultrafast MAS of 70 kHz

Federica Rossi, Nghia Tuan Duong, Manoj Kumar Pandey, Michele R. Chierotti, Roberto Gobetto, Yusuke Nishiyama

Determination of the ^{15}N chemical shift anisotropy in natural abundance samples by proton-detected 3D solid-state NMR under ultrafast MAS of 70 kHz

Magn Reson Chem. 2019; 57 pp 294–303.

DOI: 10.1002/mrc.4841

Determination of the ^{15}N chemical shift anisotropy in natural abundance samples by proton-detected 3D solid-state NMR under ultrafast MAS of 70 kHz

Federica Rossi,[a] Nghia Tuan Duong,[b] Manoj Kumar Pandey,[c] Michele R. Chierotti,[a]* Roberto Gobetto,[a] Yusuke Nishiyama[b,d,e]*

[a] Department of Chemistry and NIS Centre, University of Torino, V. P. Giuria 7, 10125, Italy.
[b] RIKEN-JEOL Collaboration Center, Yokohama, Kanagawa 230-0045, Japan
[c] Indian Institute of Technology Ropar, Nangal Road, Rupnagar 140001, Punjab, India
[d] NMR Science and Development Division, RIKEN SPring-8 Center, Yokohama, Kanagawa 230-0045, Japan

[e] JEOL RESONANCE Inc., Musashino, Akishima, Tokyo 196-8558, Japan

*Corresponding authors: (MRC) michele.chierotti@unito.it, (YN) yunishiy@jeol.co.jp

Abstract

Chemical shift anisotropy (CSA) is a sensitive probe of electronic environment at a nucleus and thus, it offers deeper insights into detailed structural and dynamics properties of different systems: e.g. chemical, biological and materials. Over the years, massive efforts have been made to develop recoupling methods that reintroduce CSA interaction under magic angle spinning (MAS) conditions. Most of them require slow or moderate MAS (≤ 20 kHz) and isotopically enriched samples. On the other hand, to the best of the authors' knowledge, no ^{13}C or ^{15}N CSA recoupling schemes at ultrafast MAS (≥60 kHz) suitable for cost-effective natural abundant samples have been developed. We present here a proton-detected 3D ^{15}N CS/^{15}N CSA/^{1}H CS correlation experiment which employs ^{1}H indirect detection for sensitivity enhancement and a γ-encoded RN_n^ν-symmetry based CSA recoupling scheme. In particular, two different symmetries, i.e. $R8^3_7$ and $R10^4_9$, are first tested, in a 2D ^{15}N CSA/^{1}H CS version, on [U-^{15}N]-L-histidine·HCl·H_2O as a model sample under 70 kHz MAS. Then the 3D experiment is applied on glycyl-L-alanine at natural abundance, resulting in site-resolved ^{15}N CSA lineshapes from which CSA parameters are retrieved by SIMPSON numerical fittings. We demonstrate that this 3D R-symmetry based pulse sequence is highly robust with respect to wide-range offset mismatches and weakly dependent to rf inhomogeneity within mis-sets of ±10% from the theoretical value.

Key words: solid-state NMR; fast MAS; ^{15}N CSA; natural abundance

Introduction

Since the advent of magic angle spinning (MAS), solid-state NMR spectroscopy has proved to be a powerful technique to investigate molecular structures and dynamics. In fact, orientation-dependent spin interactions, such as dipolar coupling and chemical shift anisotropy (CSA), are averaged out under sufficiently fast MAS rates, leading to much narrower peaks. This results in significantly improved sensitivity and resolution which in turn eases the analysis and interpretation of the spectra. However, the averaging of CSA leads to a loss of important information about conformation, molecular structure, and inter- and intramolecular hydrogen bonding, which is essential to get deeper insights on systems like proteins, drugs and materials. Hence, during the years, a large number of different approaches have been developed to firstly

recouple ^{13}C and ^{15}N CSA in the indirect dimension without sacrificing the valuable benefits provided by MAS in the direct dimension.[1–9] The whole idea behind the recoupling is to make use of a synchronized radio frequency (rf) field irradiation which would interfere with MAS averaging. For the vast majority, the current recoupling methods perform best at slow or moderate MAS rates (≤ 20 kHz) employing high rf fields such that effective recoupling is achieved. The recent introduction of probes that can reach stunningly high spinning speeds up to 110 kHz has considerably contributed to significant improvements in solid-state NMR. Besides additional enhancement in sensitivity and resolution thanks to efficiently suppressed homonuclear ^{1}H-^{1}H dipolar interaction, ultrafast MAS regime allows the practical use of 'solution-like' proton-detected correlation experiments, making measurements on cost-effective natural abundance samples possible.[10–19] Moreover, since such high rates can be achieved by notably reducing the diameter of the rotor and the volume of sample within it, this simplifies the analyses on systems for which large amounts are not feasible or difficult to obtain. Several examples can be found in site-specific ^{1}H CSA measurement by novel 2D/3D proton-detected recoupling sequences under such spinning regime.[20–24] However, to our best knowledge, no ^{13}C and ^{15}N CSA recoupling sequence for ultrafast MAS regime ≥ 60 kHz is available. In fact, being the rf field strength proportional to the spinning rate, the application of the currently available CSA recoupling schemes would lead to totally impracticable rf values when reaching speeds of 70 kHz or faster. Here, we present a proton-detected 3D ^{15}N CS/^{15}N CSA/^{1}H CS correlation experiment in which a $\mathbf{RN}_n^\nu$ recoupling scheme is applied to recouple ^{15}N CSA under ultrafast MAS. In this sequence, we took advantage of the higher sensitivity provided by the proton indirect detection. The sequence was first demonstrated on [U-^{15}N]-L-histidine·HCl·H_2O (^{15}N-L-his) as a model sample and successfully applied to glycyl-L-alanine (GlyAla) at natural abundance. ^{15}N CSA parameters are determined by numerically fitting the ^{15}N CSA experimental powder patterns which were extracted from the 3D spectra.

Design of ^{15}N CSA recoupling sequence

In the present work, we use a rotor-synchronized symmetry-based $\mathbf{RN}_n^\nu$ sequence for ^{15}N CSA recoupling,[25] where integer symmetry numbers, N, n, and ν indicate which terms are symmetrically forbidden, i.e. decoupled. The RN scheme consists of a phase alternated inversion element R_ϕ between $\pm\pi\nu/N$ each of which provides a net 180° rotation in the absence of nuclear interactions other than rf fields. The sequence spans a total of n rotor periods (τ_r), such that each inversion element has a duration of $n\tau_r/N$. First, we choose the symmetry numbers for the γ-encoded CSA recoupling of $\{\ell, m, \lambda, \mu\}=\{2, \pm1, 1, \pm1\}$ where ℓ and λ are the spatial and spin rank number of the tensorial interaction, respectively. All the other terms except for {0, 0, 0, 0} should be symmetrically forbidden. Besides the symmetry numbers, the choice of the inversion pulse element could play a significant role in the performances of the sequence. We examined symmetry-based sequences with both an inversion element of a 180° rectangular pulse and a $270°_0$-$90°_{180}$ composite-180° pulse. The symmetry numbers are selected so that rf field amplitude ($N\nu_r/2n$ and $N\nu_r/n$ for the 180° and for the 270°-90° pulse, respectively) is smaller than $1.5\nu_r$ suitable to ultrafast MAS applications. The list of symmetries is shown in Table S1. We also calculated the scaling factors and chose the symmetries with $|\kappa_{lm\lambda\mu}| > 0.2$ (highlighted in green in Table S1)[26].

Robustness with respect to rf field inhomogeneity is evaluated for each sequence by SIMPSON numerical simulations and the spectra are shown in Figure 1. Gaussian distribution is assumed for rf field distribution. It is evident that schemes with an element of 270°-90° composite-180°

pulses are more robust towards rf inhomogeneity than those with 180° rectangular pulses. $R8_7^3$ and $R10_9^4$ with a 270°-90° element outperform the others in terms of robustness towards rf inhomogeneity and thus were chosen for this study. The two $\mathbf{RN}_n^\nu$ sequences are summarized in Scheme 1 and the rf field strengths ($N\nu_r/n$) and the phases ($\pm\pi\nu/N$) of the R_ϕ block are determined by the symmetry properties for each sequence used. All parameters are listed in Table 1. The rf field strength converges in a realistic value even at ultrafast MAS conditions, as it is 1.11-1.14 times the MAS frequency.

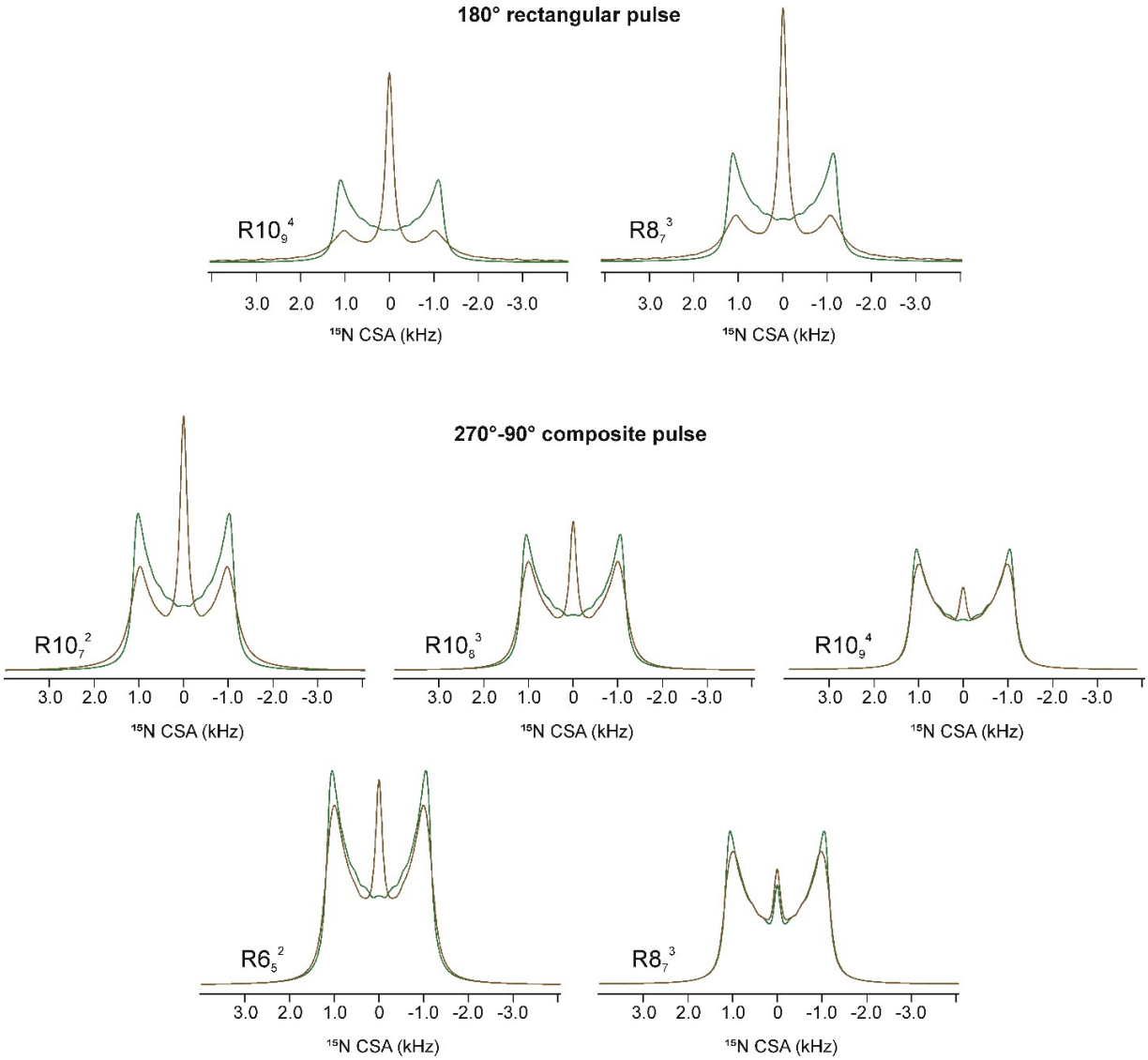

Figure 1. Recoupled ^{15}N CSA line shapes generated from SIMPSON simulations using symmetry-based $R8_7^3$ and $R10_9^4$ with a series of phase-alternating 180° pulses and $R10_7^2$, $R10_8^3$, $R10_9^4$, $R6_5^2$ and $R8_7^3$ with a series of phase-alternating $270°_0$-$90°_{180}$ composite-180° pulses having a scaling factor $|\kappa_{lm\lambda\mu}| > 0.2$ in the absence (green) and presence (brown) of rf field inhomogeneity.

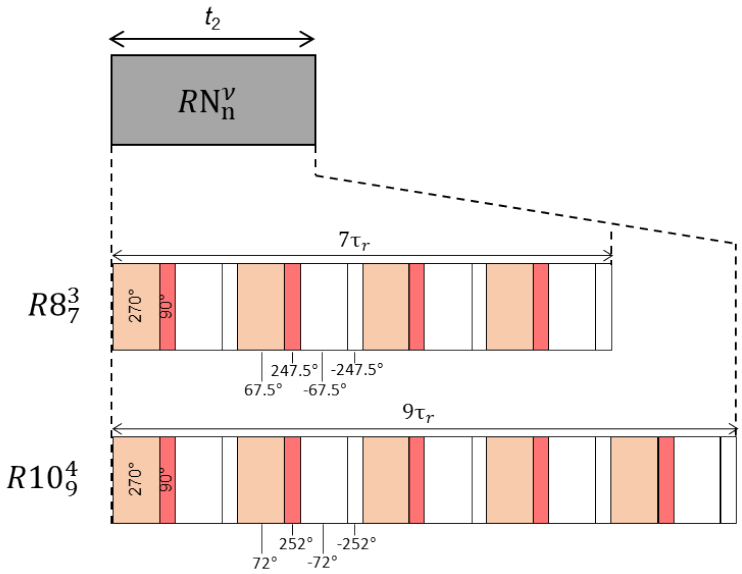

Scheme 1. $R8_7^3$ and $R10_9^4$ symmetry-based pulse sequences to record proton-detected 3D ^{15}N CS/^{15}N CSA/^{1}H CS correlation experiment at ultrafast MAS. Both consist of a series of 270°-90° pulses with phases alternating between (67.5°, 247.5°) (filled rectangles) and (-67.5°, -247.5°) (unfilled rectangles) for $R8_7^3$ and between (72°, 252°) (filled rectangles) and (-72°, -252°) (unfilled rectangles) for $R10_9^4$.

Table 1. Parameters associated with the used γ-encoded symmetry-based sequences.

Symmetry sequence	N, n, ν	R_ϕ	R'_ϕ	RF amplitude/ν_r
$R8_7^3$	8, 7, 3	$270_{67.5}90_{247.5}$	$270_{-67.5}90_{-247.5}$	1.14
$R10_9^4$	10, 9, 4	$270_{72}90_{252}$	$270_{-72}90_{-252}$	1.11

Pulse sequence

Scheme 2 shows the pulse sequence used for the proton-detected 3D ^{15}N CS/^{15}N CSA/^{1}H CS correlation experiment. Firstly, the ^{15}N magnetization is prepared by a ramped-amplitude cross-polarization (RAMP-CP) and evolves with isotropic chemical shifts during t_1 under ^{1}H decoupling. The resultant ^{15}N magnetization is stored along the z-axis by the first ^{15}N 90° pulse, allowing time-evolution under the symmetry-based RN_n^ν recoupling scheme. During the t_2 period, the net ^{15}N magnetization is allowed to evolve along the z axis with the recoupled ^{15}N CSA. ^{15}N-^{1}H heteronuclear low-power CW decoupling is applied throughout these periods (t_1 and t_2) on the ^{1}H channel. The residual ^{1}H magnetization is removed by homonuclear rotary resonance (HORROR) prior to the second CP from ^{15}N to ^{1}H. Finally, ^{1}H spectra are acquired under ^{15}N-^{1}H WALTZ decoupling on the ^{15}N channel.

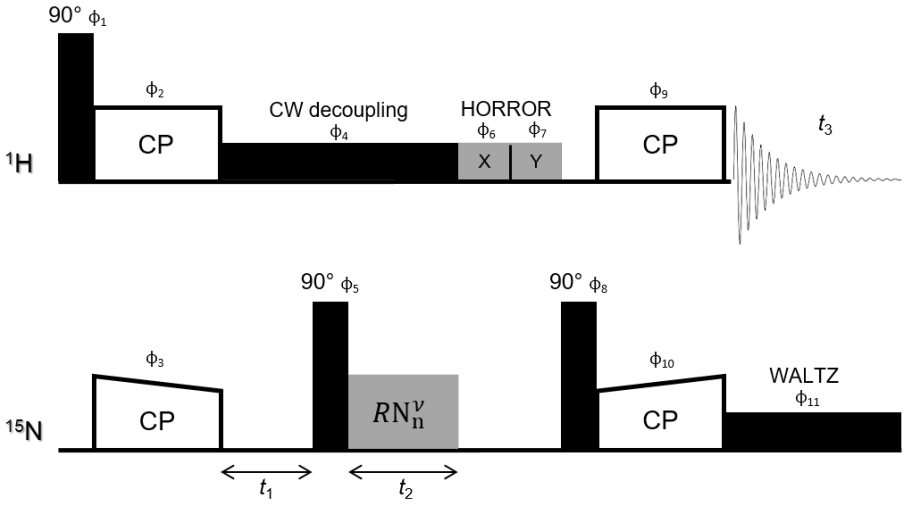

Scheme 2. Proton-detected 3D ^{15}N CS/^{15}N CSA/^{1}H CS pulse sequence. During t_1, ^{15}N isotropic chemical shifts are expressed under the ^{1}H CW decoupling, whereas ^{15}N CSA is recoupled during t_2. The phase cycling scheme used in the 3D pulse sequence is as follows: ϕ_1={4 (0), 4 (180)}, ϕ_2={90}, ϕ_3={0, 180}, ϕ_4={0}, ϕ_5={90}, ϕ_6={0}, ϕ_7={90}, ϕ_8={270}, ϕ_9={2 (0), 2 (180)}, ϕ_{10}={0}, ϕ_{11}={0}, ϕ_{acq}={0, 180, 180, 0, 180, 0, 0, 180}.

Material and methods

^{15}N-L-his and natural abundance GlyAla were purchased from Aldrich and used without further purification. All NMR experiments were performed on a solid-state NMR spectrometer (JNM-ECZ900R, JEOL RESONANCE Inc., Japan) equipped with a 1.0 mm triple-resonance ultrafast MAS probe (JEOL RESONANCE Inc., Japan), operating at ^{1}H and ^{15}N Larmor frequencies of 899.44 and 91.14 MHz, respectively, at a magnetic field of 21.1 T. Samples were separately packed in cylindrical 1 mm o.d. zirconia rotors. All measurements were acquired at ambient temperature under 70 kHz MAS. The ^{1}H and ^{15}N 90° pulse lengths were set to 0.97 and 2.2 µs, respectively. Recycle delays of 8 and 3 s for L-His and GlyAla, respectively and a ^{1}H acquisition length of 8.19 ms were used in all experiments. For the 3D experiment 32 transients were collected for each 24 t_1 and 16 t_2 increments, whereas in the 2D ^{15}N CSA/^{1}H CS version 8 transients were collected for each 12 t_2 increments. A contact time of 2 ms was used for the first CP (^{1}H to ^{15}N) to maximize the magnetization transfer efficiency, whereas a short contact time of 0.3 ms was used for the second CP (^{15}N to ^{1}H) to select only those protons covalently bonded to nitrogen. rf fields strengths of 15 and 55 kHz were used for ^{1}H and ^{15}N, respectively to fulfill the double quantum Hartmann-Hahn condition in both CP steps. The phase-alternated HORROR sequence was applied for 50 ms with 35 kHz ^{1}H rf field. During the t_1 and t_2 periods, a ^{15}N-^{1}H heteronuclear continuous-wave (CW) decoupling of 38.6 for $R10_9^4$ or 41.2 kHz for $R8_7^3$ was applied on the ^{1}H channel, whereas during the t_3 acquisition period a ^{15}N-^{1}H WALTZ decoupling with rf field strength of 12.9 kHz and nominal 90 degree pulse length of 25 µs was applied on the ^{15}N channel.

All the NMR data were processed using Delta NMR software (JEOL RESONANCE Inc.). t_1, t_2 and t_3 dimensions were processed by the application of zero filling followed by Fourier transformation. The CSA parameters were retrieved by numerical fittings using SIMPSON program.[27] Powder averaging was achieved using 10 Euler γ-angles and 2000 α/β angles

employing the REPULSION method for powder averaging.[28] CSA parameters are reported according to the Haeberlen convention where: principal components: $|\delta_{zz} - \delta_{iso}| \geq |\delta_{xx} - \delta_{iso}| \geq |\delta_{yy} - \delta_{iso}|$; isotropic value: $\delta_{iso} = (\delta_{11} + \delta_{22} + \delta_{33})/3$; reduced anisotropy: $\delta_{aniso} = \delta_{zz} - \delta_{iso}$; anisotropy: $\Delta\sigma = \delta_{zz} - (\delta_{xx} + \delta_{yy})/2$; asymmetry: $\eta = (\delta_{yy} - \delta_{xx}) / \delta_{aniso}$; $(0 \leq \eta \leq +1)$.

Results and discussion/Experimental verification

First, we demonstrated the experimental setup and performance of the $R8_7^3$ and $R10_9^4$ sequences on ^{15}N-L-his as model sample (Scheme 3).

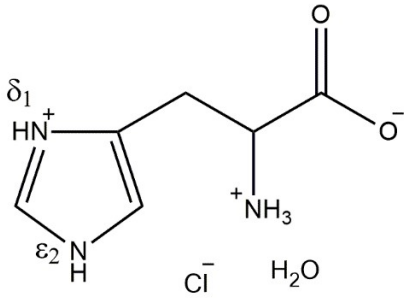

Scheme 3. Chemical structure of L-histidine·HCl·H_2O.

Fortunately, the three proton resonances of NH_3^+, NH and NH^+ groups are well resolved in the proton dimension, thus the ^{15}N CSA line shape for each nitrogen site can be extracted with the 2D ^{15}N CSA/^{1}H CS experiment (Scheme 2 with t_1=0) rather than the time-consuming 3D measurement. The spectrum observed with the $R10_9^4$ symmetry provides ^{15}N CSA powder patterns in the indirect dimension (Figure 2). Similar result was also obtained by employing the other symmetry, i.e. $R8_7^3$ (Figure S1).

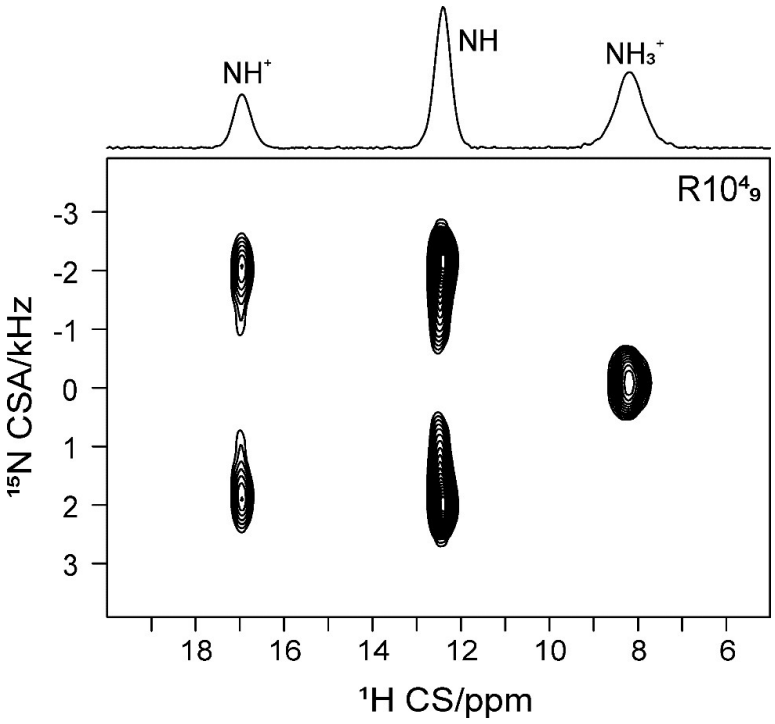

Figure 2. 2D ^{15}N CSA/^{1}H CS correlation spectrum (^{1}H = 899.4 MHz, ^{15}N = 91.1 MHz) of ^{15}N-L-his recorded at MAS of 70 kHz using symmetry-based $R10_9^4$ pulse sequence. Measurement time is ~ 30 minutes.

It should be noted that ^{15}N CSA and ^{1}H-^{15}N heteronuclear dipolar interaction possess the same spin and spatial symmetry in case of a single rf channel irradiation and thus, are recoupled simultaneously. Hence, heteronuclear decoupling during the ^{15}N CSA recoupling period is required. However, optimization of ^{1}H decoupling is not straightforward as it may reintroduce ^{1}H-^{15}N dipolar interaction. Firstly, a comparison between CW and WALTZ decoupling, which is optimized by ^{15}N CPMAS experiments, during the recoupling time was carried out for both $R8_7^3$ and $R10_9^4$ schemes (Figure S2(a)). It is clearly shown that CW outperforms WALTZ. This is most probably due to interference between the WALTZ phase modulation and the RN recoupling sequence. Further optimization of CW decoupling was performed on the ^{15}N CSA dimension at various ^{1}H rf field strengths and the best line shape (highest signal intensity) is obtained at 38.6 kHz CW decoupling for the $R10_9^4$ symmetry (Figure S2(b)). The condition is close to the HORROR condition and reintroduces ^{1}H-^{1}H dipolar interaction, which enhances the decoupling efficiency of the ^{1}H-^{15}N heteronuclear dipolar coupling. The SIMPSON simulations carried out on a spin system with and without ^{1}H-^{15}N dipolar interactions and with and without CW decoupling along with the experimental spectrum are shown in Figure 3. The numerical simulation well reproduces the experimental observation. It is also affirmed that no visible effect of ^{1}H-^{15}N dipolar interaction remains at the optimal ^{1}H decoupling conditions. In fact, in the absence of a suitable ^{1}H decoupling, the resulting powder patterns would contain the contribution of both the ^{15}N CSA and ^{1}H-^{15}N dipolar coupling, leading to complex line shapes and preventing the accurate CSA measurement.

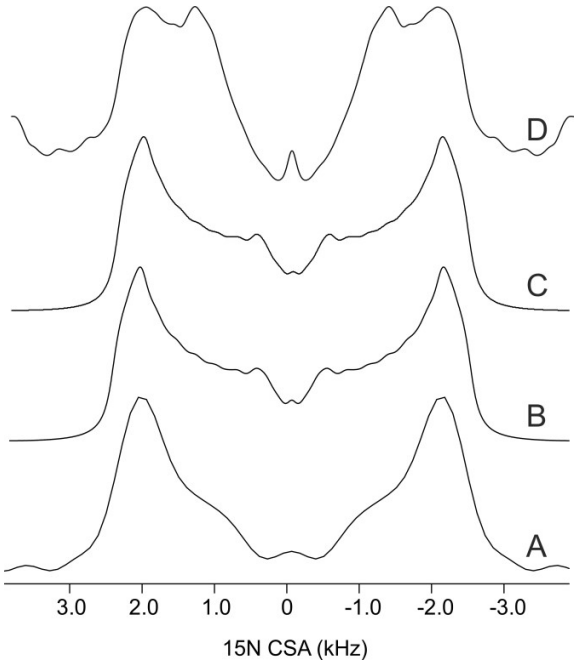

Figure 3. Experimental ^{15}N CSA line shape of the $N_{\varepsilon 2}$-H group of ^{15}N-L-his (A), along with SIMPSON simulations carried out on: a single nitrogen spin (i.e. without ^{1}H-^{15}N dipolar

interactions) (B); with ^{1}H-^{15}N dipolar interactions under optimum CW decoupling (C); and with ^{1}H-^{15}N dipolar interactions without CW decoupling (D).

In order to extract accurate CSA parameters from powder pattern in the indirect dimension, root mean square deviation (RMSD) analysis was carried out by simulating several spectra with different combinations of δ_{aniso} and η values (Figure 4). The symmetry-based sequence appears insensitive to asymmetry parameter changes, whereas quite reliable for anisotropy.

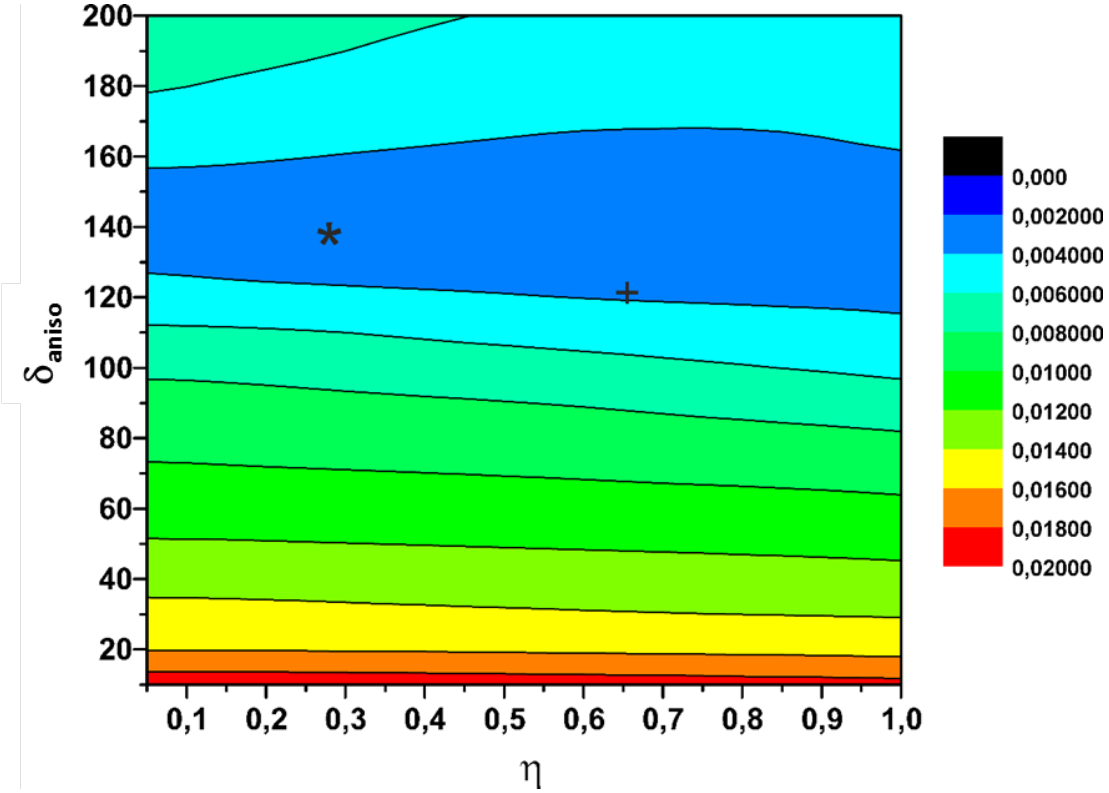

Figure 4. RMSD values plotted as function of anisotropy, $\delta_{aniso,}$ and asymmetry, η, for the $N_{\varepsilon 2}$-H group of ^{15}N-L-his. The asterisk indicates the value found by the application of the RN sequence; the plus symbol marks off the value obtained from the Herzfeld-Berger analysis on SSBs at slow MAS.

Figure 5 shows the $R10_9^4$ experimental ^{15}N CSA line shape (black line) extracted from the spectral slice at ^{1}H chemical shift of 12.4 ppm ($N_{\varepsilon 2}$-H group) and best numerical fitting for ^{15}N CSA parameters of anisotropy, δ_{aniso} = 140.0 ppm and asymmetry, η = 0.25 (shown in Figure 4 by *). However, as shown in the RMSD plot, the asymmetry parameter can include significant error.

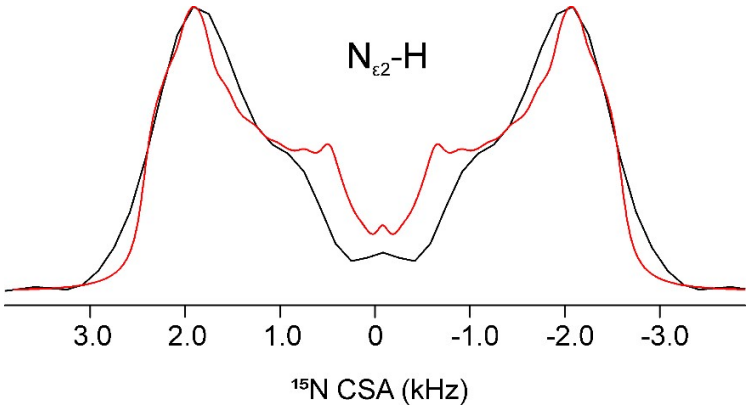

Figure 5. Experimental ^{15}N CSA line shape (black line) extracted by taking a slice parallel to ^{15}N CSA dimension at the ^{15}N isotropic chemical shift of the $N_{\varepsilon 2}$-H group from the 2D spectrum of ^{15}N-L-his employing $R10_9^4$, along with best fitting simulated line shape (red line) obtained using SIMPSON program.

We also carried out the Herzfeld-Berger analysis on spinning sidebands (SSBs) of a ^{15}N CPMAS spectrum at slow MAS rate (about 2 kHz). The CSA values are determined as δ_{aniso} = -123.4 ppm and η = 0.66 for the group $N_{\varepsilon 2}$-H (shown in Figure 4 by +) and δ_{aniso} = -126.5 ppm and η = 0.28 for the $N_{\delta 1}$-H, which are good agreement with the literature values of δ_{aniso} = -118.0 ppm and η = 0.69 and δ_{aniso} = -125.8 ppm and η = 0.56, respectively.[29] Although large discrepancies are found in the asymmetry parameter, the good agreement is obtained in the anisotropies. The CSA parameters of $N_{\delta 1}$-H (δ_{aniso} = 139.0 and η = 0.37) found with the new sequence are also demonstrated in Figure S3, which also show good agreement with those found by SSB analysis on the ^{15}N CPMAS spectrum acquired at slow MAS rates. It should be noted that the sign of anisotropy cannot be determined by the current method. This limitation comes from recoupling terms only with $|m|$ = 1, which results in two possible combinations of eigenvalues of the CSA tensor. Sign discrimination can be achieved by simultaneously recoupling two terms with $|m|$ = 1 and 2.

To evaluate the robustness of the pulse sequence with respect to rf inhomogeneity/mismatching, the ^{15}N CSA lineshapes were observed at rf amplitudes deliberately mis-set from the theoretical value, using both symmetries $R8_7^3$ and $R10_5^4$ (Figure 6). It is found that the RN-based pulse sequence is tolerant of mis-sets of approximately ±10% from the theoretical rf amplitude.

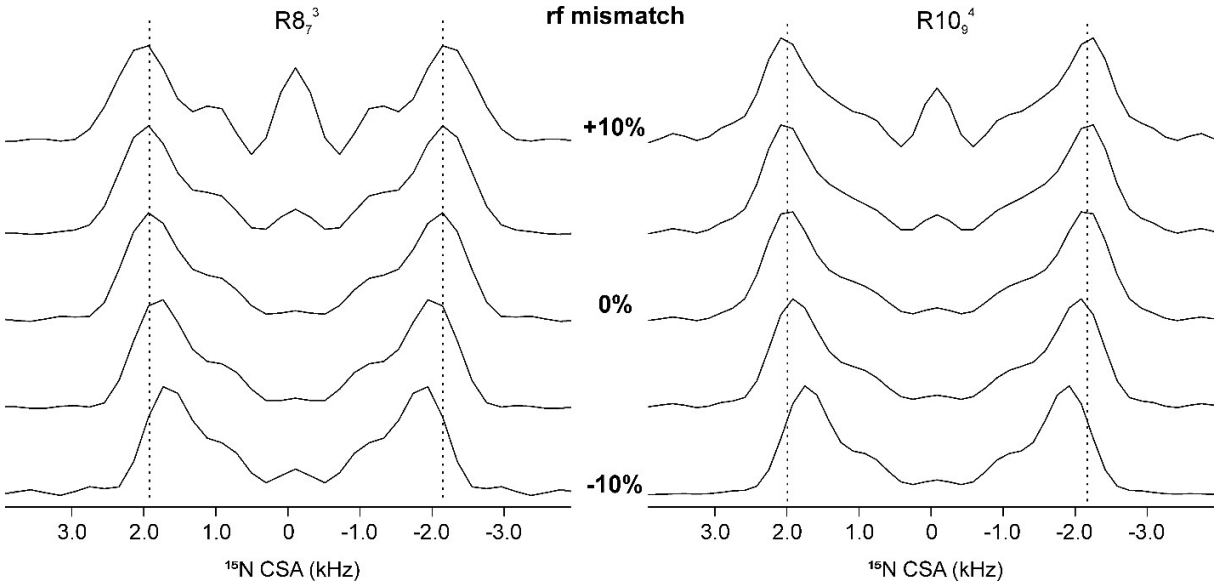

Figure 6. Experimental ^{15}N CSA line shapes of the $N_{\varepsilon 2}$-H group of ^{15}N-L-his as a function of rf amplitude mismatch (±10%) from the theoretical value, using $R8_7^3$ and $R10_9^4$ symmetry-based sequences.

Moreover, as the ^{15}N resonances can assume several different chemical shifts in the ^{15}N dimension (up to 300 ppm), the sequence should be robust with respect to ^{15}N offset. The effect is experimentally demonstrated. As the isotropic chemical shift is symmetrically forbidden, the resonance offset is absent in the first order. No visible deviations on ^{15}N CSA line shapes is observed in the 40-180 ppm chemical shift range (Figure 7).

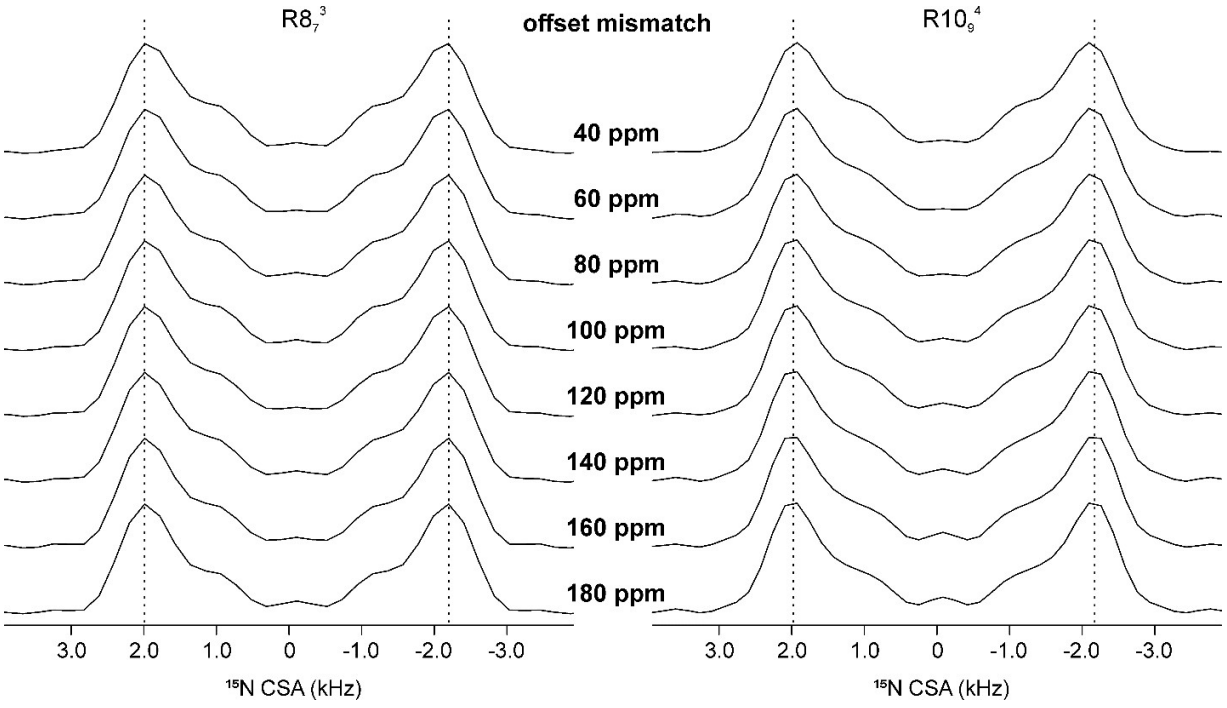

Figure 7. Experimental ^{15}N CSA line shapes of the $N_{\varepsilon 2}$-H group of ^{15}N-L-his as a function of resonance offset mismatch (range 40–180 ppm), using $R8_7^3$ and $R10_9^4$ symmetry-based sequences.

Subsequently, we applied the ^{15}N CSA recoupling sequences on a challenging sample, GlyAla at natural abundance (Scheme 4).

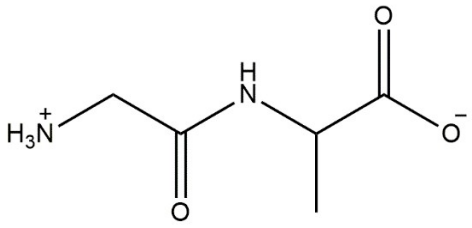

Scheme 4. Chemical structure of glycyl-L-alanine.

In addition to low sensitivity, which is attributed to the low natural abundance of ^{15}N (0.37%), the possible presence of overlapped NH resonances in the ^{1}H dimension poses an additional difficulty. In fact, the NH resonances often overlap to each other as the chemical shift range of amide proton is limited. In this case, the proton detection and a ^{15}N isotropic chemical shift dimension (third dimension) are essential to acquire site-specific ^{15}N signal with enhanced signal to noise (S/N) ratio, allowing observation of naturally abundant samples. The 3D ^{15}N CS/^{15}N CSA/^{1}H CS experiments with both $R8_7^3$ and $R10_9^4$ were successfully measured on GlyAla (Figure 8 for R10, and Figures S4, S5 and S6 for R8).

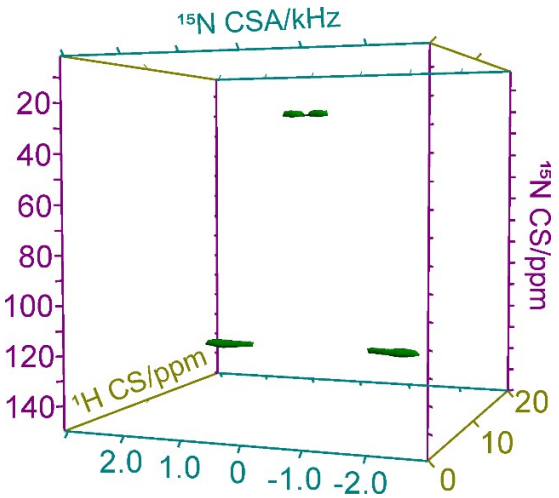

Figure 8. 3D ^{15}N CS/^{15}N CSA/^{1}H CS correlation spectrum (^{1}H = 899.4 MHz, ^{15}N = 91.1 MHz) of GlyAla recorded at MAS of 70 kHz using symmetry-based $R10_9^4$ pulse sequence. Measurement time is ~ 28 hours.

From the extracted ^{15}N CSA/^{1}H CS 2D spectrum (Figure 9), it is clear that the third dimension in which ^{15}N isotropic chemical shift is expressed is not strictly necessary for this sample. In fact, the two ^{1}H peaks are partially overlapped but can still be discriminated, allowing the extraction of ^{15}N CSA line shapes, for both NH and NH_3^+ groups.

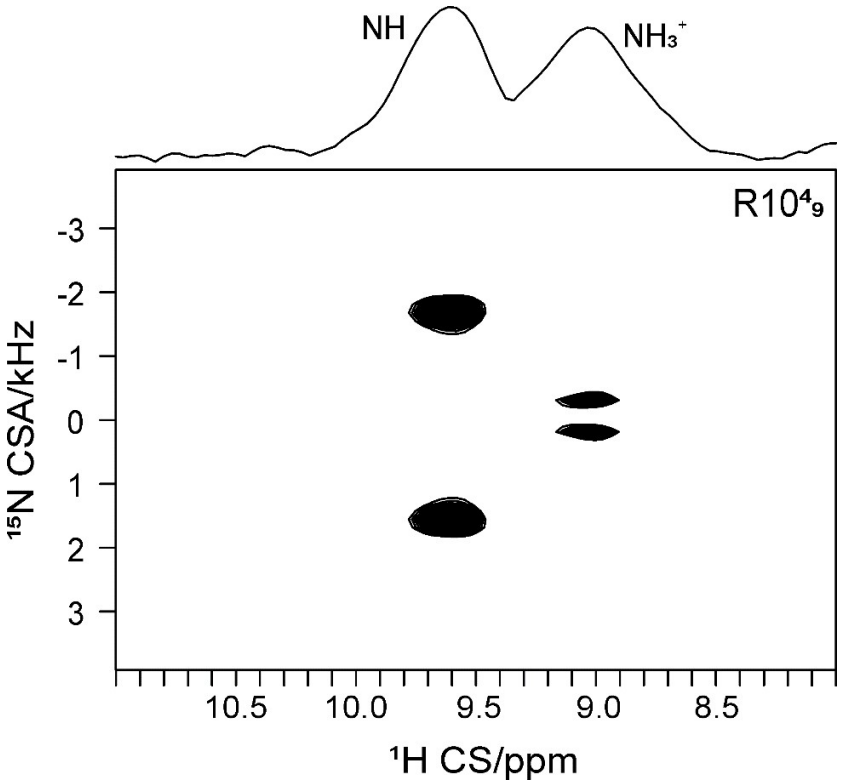

Figure 9. 2D ^{15}N CSA/^{1}H CS correlation spectrum (^{1}H = 899.4 MHz, ^{15}N = 91.1 MHz) of GlyAla recorded at MAS of 70 kHz using symmetry-based $R10_9^4$ pulse sequence. Measurement time is for the 3D is ~ 28 hours.

However, the third dimension would become essential for samples which show strongly overlapped ^{1}H signals, preventing the distinction of different sites. Additionally, by extracting the 2D ^{15}N CSA/^{1}H CS spectrum, ^{1}H isotropic chemical shifts are more precisely determined and can be used for basic molecular assignment and/or structural refinement in quantum chemical calculations. An alternative approach would be to perform a quick 2D ^{1}H-^{15}N HETCOR spectrum to locate the ^{15}N isotropic chemical shifts and then a set of 2D ^{15}N CSA/^{1}H CS recoupling experiments with frequency selective ^{15}N pulses to measure CSA for the nitrogen signals of interest. This is particularly useful if no resonance overlaps are observed in the ^{15}N dimensions. To determine the ^{15}N CSA parameters from the 3D spectrum of GlyAla (Figure 8), the 2D ^{15}N CS/^{15}N CSA projection (Figure 10) was extracted, in which two nitrogen sites with significantly different CSA values are observed.

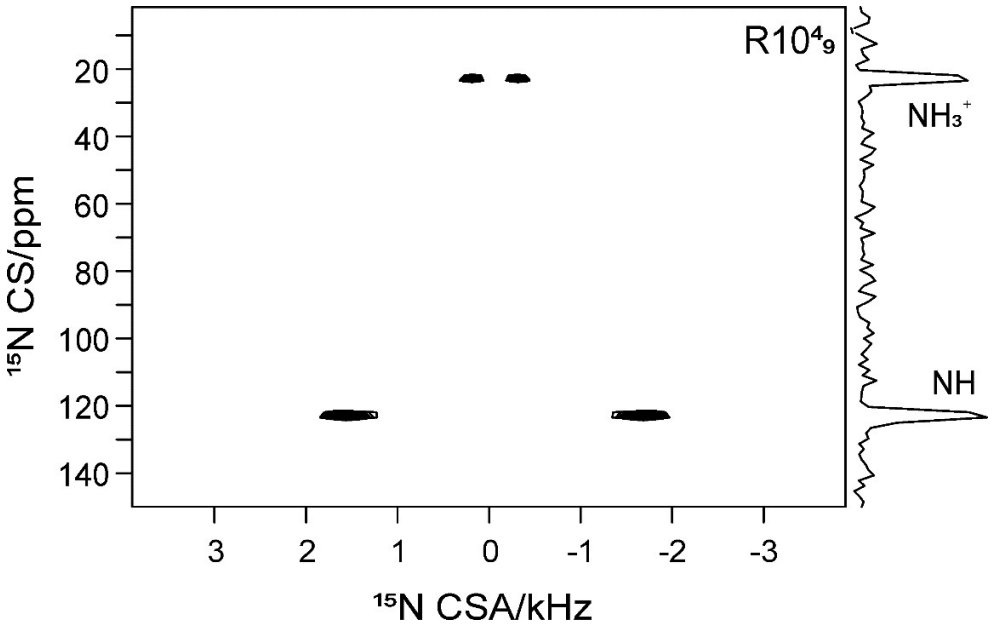

Figure 10. 2D projected ^{15}N CS/^{15}N CSA correlation spectrum (^{1}H = 899.4 MHz, ^{15}N = 91.1 MHz) of GlyAla recorded at MAS of 70 kHz using symmetry-based $R10_9^4$ pulse sequence. Measurement time for the 3D is ~ 28 hours.

The experimental NH_3^+ and NH ^{15}N CSA line shapes (black lines in Figure 11) were extracted by taking the corresponding spectral slices parallel to CSA dimension at the ^{15}N isotropic chemical shifts of 22.5 and 122.7 ppm, respectively. A well resolved 'Pake-like' peak shape is observed for the ^{15}N CSA of the NH group, whereas the NH_3^+ group shows a small ^{15}N CSA in agreement with its high local spherical symmetry.
Finally, the best fits of the experimental ^{15}N CSA line shapes (red lines in Figure 11) were achieved by simulations with SIMPSON and the obtained parameters, namely isotropic chemical shift δ_{iso}, anisotropy, δ_{aniso} and asymmetry, η are listed in Table 2. It should be noted that large error in asymmetry parameter is possible.

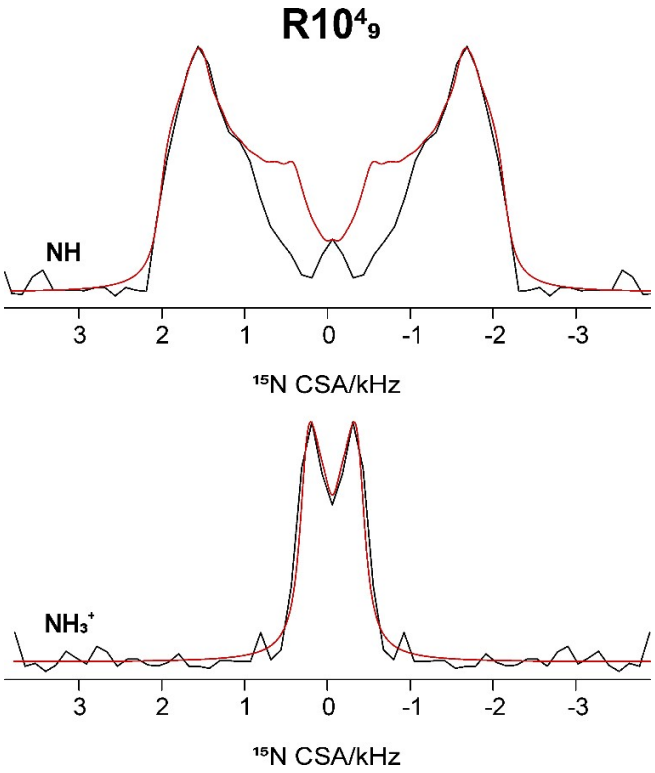

Figure 11. ^{15}N CSA experimental line shapes (black lines) extracted by taking the slices parallel to anisotropic dimension at ^{15}N chemical shift of the NH and NH_3^+ groups of GlyAla from Fig. 10 and SIMPSON best fitting simulated line shapes (red lines) to extract ^{15}N CSA parameters.

Table 2. ^{15}N CSA parameters obtained by fitting the experimental line shapes for GlyAla using $R8_7^3$ and $R10_9^4$.

Symmetry	NH_3^+			NH		
	δ_{iso}	δ_{aniso}	η	δ_{iso}	δ_{aniso}	η
$R8_7^3$	22.8	21.0	0.40	122.9	112.0	0.25
$R10_9^4$	22.8	20.0	0.30	122.9	112.0	0.38

The experimental parameters obtained through the application of the $R8_7^3$ and $R10_9^4$ schemes are in good agreement with literature and show how this novel pulse sequence can be effectively applied to ^{15}N CSA recoupling in natural abundance samples.

Conclusions

In summary, we have presented a proton-detected 3D ^{15}N CS/^{15}N CSA/^{1}H CS correlation experiment to recouple ^{15}N CSA in natural abundance samples at ultrafast MAS of 70 kHz. Specifically, two γ-encoded RN_n^ν-symmetries, i.e. $R8_7^3$ and $R10_9^4$, were discussed and proved to be very robust towards mismatches of both rf field amplitude and resonance offset. The

sequences were successfully applied to natural abundance glycyl-L-alanine and allowed for a site-resolved ^{15}N CSA parameters determination. In particular, the anisotropy, δ_{aniso} and the asymmetry, η values were retrieved by fitting the ^{15}N CSA experimental line shapes with SIMPSON. We believe that the pulse sequences presented in this study represent an interesting improvement to the current ^{15}N CSA recoupling sequences which fail at such ultra-fast spinning speeds and more when dealing with natural abundance samples. The challenging purpose to extend such CSA measurements to natural abundance systems was achieved by exploiting the proton-detection method, feasible only at very high spinning rates, which significantly improves the S/N ratio of low abundant nuclei, such as ^{15}N. It should be noted that because of amplitude-modulated signal in the CSA dimension, the γ-encoded sequence fails to determine the sign of anisotropy. The simultaneous recoupling of m=$\pm$1, $\pm$2 terms in non γ-encoded form may solve the problem. This may improve the sensitivity to asymmetry parameters. We are now working on it.

References

(1) Wei, Y.; Lee, D.-K.; McDermott, A. E.; Ramamoorthy, A. A 2D MAS Solid-State NMR Method to Recover the Amplified Heteronuclear Dipolar and Chemical Shift Anisotropic Interactions. *Journal of Magnetic Resonance* **2002**, *158* (1), 23–35. https://doi.org/10.1016/S1090-7807(02)00056-3.

(2) Chan, J. C. C.; Tycko, R. Recoupling of Chemical Shift Anisotropies in Solid-State NMR under High-Speed Magic-Angle Spinning and in Uniformly 13C-Labeled Systems. *The Journal of Chemical Physics* **2003**, *118* (18), 8378–8389. https://doi.org/10.1063/1.1565109.

(3) Eléna, B.; Hediger, S.; Emsley, L. Correlation of Fast and Slow Chemical Shift Spinning Sideband Patterns under Fast Magic-Angle Spinning. *Journal of Magnetic Resonance* **2003**, *160* (1), 40–46. https://doi.org/10.1016/S1090-7807(02)00037-X.

(4) Shao, L.; Crockford, C.; Geen, H.; Grasso, G.; Titman, J. J. Chemical Shift Anisotropy Amplification. *Journal of Magnetic Resonance* **2004**, *167* (1), 75–86. https://doi.org/10.1016/j.jmr.2003.11.005.

(5) Wylie, B. J.; Franks, W. T.; Rienstra, C. M. Determinations of 15N Chemical Shift Anisotropy Magnitudes in a Uniformly 15N,13C-Labeled Microcrystalline Protein by Three-Dimensional Magic-Angle Spinning Nuclear Magnetic Resonance Spectroscopy. *J. Phys. Chem. B* **2006**, *110* (22), 10926–10936. https://doi.org/10.1021/jp060507h.

(6) Shao, L.; Crockford, C.; Titman, J. J. Chemical Shift Anisotropy Amplification with High Amplification Factor and Improved Sensitivity. *Journal of Magnetic Resonance* **2006**, *178* (1), 155–161. https://doi.org/10.1016/j.jmr.2005.10.005.

(7) Hou, G.; Paramasivam, S.; Byeon, I.-J. L.; Gronenborn, A. M.; Polenova, T. Determination of Relative Tensor Orientations by γ-Encoded Chemical Shift Anisotropy/Heteronuclear Dipolar Coupling 3D NMR Spectroscopy in Biological Solids. *Phys. Chem. Chem. Phys.* **2010**, *12* (45), 14873–14883. https://doi.org/10.1039/C0CP00795A.

(8) Hou, G.; Byeon, I.-J. L.; Ahn, J.; Gronenborn, A. M.; Polenova, T. Recoupling of Chemical Shift Anisotropy by R-Symmetry Sequences in Magic Angle Spinning NMR Spectroscopy. *The Journal of Chemical Physics* **2012**, *137* (13), 134201. https://doi.org/10.1063/1.4754149.

(9) Paramasivam, S.; Gronenborn, A. M.; Polenova, T. Backbone Amide 15N Chemical Shift Tensors Report on Hydrogen Bonding Interactions in Proteins: A Magic Angle Spinning NMR Study. *Solid State Nuclear Magnetic Resonance* **2018**, *92*, 1–6. https://doi.org/10.1016/j.ssnmr.2018.03.002.

(10) Tatton, A. S.; Bradley, J. P.; Iuga, D.; Brown, S. P. 14N–1H Heteronuclear Multiple-Quantum Correlation Magic-Angle Spinning NMR Spectroscopy of Organic Solids. *Zeitschrift für Physikalische Chemie* **2012**, *226* (11–12), 1187–1204. https://doi.org/10.1524/zpch.2012.0308.
(11) Reddy, G. N. M.; Malon, M.; Marsh, A.; Nishiyama, Y.; Brown, S. P. Fast Magic-Angle Spinning Three-Dimensional NMR Experiment for Simultaneously Probing H—H and N—H Proximities in Solids. *Anal. Chem.* **2016**, *88* (23), 11412–11419. https://doi.org/10.1021/acs.analchem.6b01869.
(12) Nishiyama, Y.; Malon, M.; Potrzebowski, M. J.; Paluch, P.; Amoureux, J. P. Accurate NMR Determination of C–H or N–H Distances for Unlabeled Molecules. *Solid State Nuclear Magnetic Resonance* **2016**, *73*, 15–21. https://doi.org/10.1016/j.ssnmr.2015.06.005.
(13) Bordignon, S.; Cerreia Vioglio, P.; Priola, E.; Voinovich, D.; Gobetto, R.; Nishiyama, Y.; Chierotti, M. R. Engineering Codrug Solid Forms: Mechanochemical Synthesis of an Indomethacin–Caffeine System. *Crystal Growth & Design* **2017**, *17* (11), 5744–5752. https://doi.org/10.1021/acs.cgd.7b00748.
(14) Rossi, F.; Cerreia Vioglio, P.; Bordignon, S.; Giorgio, V.; Nervi, C.; Priola, E.; Gobetto, R.; Yazawa, K.; Chierotti, M. R. Unraveling the Hydrogen Bond Network in a Theophylline–Pyridoxine Salt Cocrystal by a Combined X-Ray Diffraction, Solid-State NMR, and Computational Approach. *Crystal Growth & Design* **2018**, *18* (4), 2225–2233. https://doi.org/10.1021/acs.cgd.7b01662.
(15) Ishii, Y.; Tycko, R. Sensitivity Enhancement in Solid State 15N NMR by Indirect Detection with High-Speed Magic Angle Spinning. *Journal of Magnetic Resonance* **2000**, *142* (1), 199–204. https://doi.org/10.1006/jmre.1999.1976.
(16) Schnell, I.; Langer, B.; Söntjens, S. H. M.; van Genderen, M. H. P.; Sijbesma, R. P.; Spiess, H. W. Inverse Detection and Heteronuclear Editing in 1H–15N Correlation and 1H–1H Double-Quantum NMR Spectroscopy in the Solid State under Fast MAS. *Journal of Magnetic Resonance* **2001**, *150* (1), 57–70. https://doi.org/10.1006/jmre.2001.2312.
(17) Althaus, S. M.; Mao, K.; Stringer, J. A.; Kobayashi, T.; Pruski, M. Indirectly Detected Heteronuclear Correlation Solid-State NMR Spectroscopy of Naturally Abundant 15N Nuclei. *Solid State Nuclear Magnetic Resonance* **2014**, *57–58*, 17–21. https://doi.org/10.1016/j.ssnmr.2013.11.001.
(18) Zhou, D. H.; Rienstra, C. M. Rapid Analysis of Organic Compounds by Proton-Detected Heteronuclear Correlation NMR Spectroscopy with 40 KHz Magic-Angle Spinning. *Angewandte Chemie International Edition* **2008**, *47* (38), 7328–7331. https://doi.org/10.1002/anie.200802108.
(19) Wiench, J. W.; Bronnimann, C. E.; Lin, V. S.-Y.; Pruski, M. Chemical Shift Correlation NMR Spectroscopy with Indirect Detection in Fast Rotating Solids: Studies of Organically Functionalized Mesoporous Silicas. *J. Am. Chem. Soc.* **2007**, *129* (40), 12076–12077. https://doi.org/10.1021/ja074746+.
(20) Duma, L.; Abergel, D.; Tekely, P.; Bodenhausen, G. Proton Chemical Shift Anisotropy Measurements of Hydrogen-Bonded Functional Groups by Fast Magic-Angle Spinning Solid-State NMR Spectroscopy. *Chem. Commun.* **2008**, *0* (20), 2361–2363. https://doi.org/10.1039/B801154K.
(21) Pandey, M. K.; Nishiyama, Y. Determination of Relative Orientation between 1H CSA Tensors from a 3D Solid-State NMR Experiment Mediated through 1H/1H RFDR Mixing under Ultrafast MAS. *Solid State Nuclear Magnetic Resonance* **2015**, *70*, 15–20. https://doi.org/10.1016/j.ssnmr.2015.05.001.
(22) Pandey, M. K.; Malon, M.; Ramamoorthy, A.; Nishiyama, Y. Composite-180° Pulse-Based Symmetry Sequences to Recouple Proton Chemical Shift Anisotropy Tensors under

Ultrafast MAS Solid-State NMR Spectroscopy. *Journal of Magnetic Resonance* **2015**, *250*, 45–54. https://doi.org/10.1016/j.jmr.2014.11.002.
(23) Pandey, M. K.; Yarava, J. R.; Zhang, R.; Ramamoorthy, A.; Nishiyama, Y. Proton-Detected 3D 15N/1H/1H Isotropic/Anisotropic/Isotropic Chemical Shift Correlation Solid-State NMR at 70kHz MAS. *Solid State Nuclear Magnetic Resonance* **2016**, *76–77*, 1–6. https://doi.org/10.1016/j.ssnmr.2016.03.001.
(24) Miah, H. K.; Cresswell, R.; Iuga, D.; Titman, J. J. 1H CSA Parameters by Ultrafast MAS NMR: Measurement and Applications to Structure Refinement. *Solid State Nuclear Magnetic Resonance* **2017**, *87*, 67–72. https://doi.org/10.1016/j.ssnmr.2017.02.002.
(25) Levitt, M. H. Symmetry-Based Pulse Sequences in Magic-Angle Spinning Solid-State NMR. In *Encyclopedia of Nuclear Magnetic Resonance. Volume 9, Advances in NMR*; Grant, D. M., Harris, R. K., Eds.; Wiley, 2002; pp 165–196.
(26) Nishiyama, Y.; Yamazaki, T.; Terao, T. Development of Modulated Rf Sequences for Decoupling and Recoupling of Nuclear-Spin Interactions in Sample-Spinning Solid-State NMR: Application to Chemical-Shift Anisotropy Determination. *The Journal of Chemical Physics* **2006**, *124* (6), 064304. https://doi.org/10.1063/1.2141949.
(27) Bak, M.; Rasmussen, J. T.; Nielsen, N. C. SIMPSON: A General Simulation Program for Solid-State NMR Spectroscopy. *Journal of Magnetic Resonance* **2000**, *147* (2), 296–330. https://doi.org/10.1006/jmre.2000.2179.
(28) Bak, M.; Nielsen, N. C. REPULSION, A Novel Approach to Efficient Powder Averaging in Solid-State NMR. *Journal of Magnetic Resonance* **1997**, *125* (1), 132–139. https://doi.org/10.1006/jmre.1996.1087.
(29) Kalakewich, K.; Iuliucci, R.; Mueller, K. T.; Eloranta, H.; Harper, J. K. Monitoring the Refinement of Crystal Structures with 15N Solid-State NMR Shift Tensor Data. *The Journal of Chemical Physics* **2015**, *143* (19), 194702. https://doi.org/10.1063/1.4935367.